

# SEARCHES FOR QUARK AND LEPTON COMPOSITENESS

Revised 2015 by K. Hikasa (Tohoku University), M. Tanabashi (Nagoya University), K. Terashi (University of Tokyo), and N. Varelas (University of Illinois at Chicago)

## *Limits on contact interactions*

If quarks and leptons are made of constituents, then at the scale of constituent binding energies there should appear new interactions among them. At energies much below the compositeness scale ( $\Lambda$ ), these interactions are suppressed by inverse powers of  $\Lambda$ . The dominant effect of the compositeness of fermion  $\psi$  should come from the lowest dimensional interactions with four fermions (contact terms), whose most general flavor-diagonal color-singlet chirally invariant form reads [1,2]

$$\begin{aligned} \mathcal{L} = & \frac{g_{\text{contact}}^2}{2\Lambda^2} \sum_{i,j} \left[ \eta_{LL}^{ij} (\bar{\psi}_L^i \gamma_\mu \psi_L^i) (\bar{\psi}_L^j \gamma^\mu \psi_L^j) \right. \\ & + \eta_{RR}^{ij} (\bar{\psi}_R^i \gamma_\mu \psi_R^i) (\bar{\psi}_R^j \gamma^\mu \psi_R^j) + \eta_{LR}^{ij} (\bar{\psi}_L^i \gamma_\mu \psi_L^i) (\bar{\psi}_R^j \gamma^\mu \psi_R^j) \\ & \left. + \eta_{RL}^{ij} (\bar{\psi}_R^i \gamma_\mu \psi_R^i) (\bar{\psi}_L^j \gamma^\mu \psi_L^j) \right] , \end{aligned} \quad (1)$$

with  $i, j$  being the indices of fermion species. Color and other indices are suppressed in Eq. (1). Chiral invariance provides a natural explanation why quark and lepton masses are much smaller than their inverse size  $\Lambda$ . Note  $\eta_{\alpha\beta}^{ij} = \eta_{\beta\alpha}^{ji}$ , therefore, in order to specify the contact interaction among the same fermion species  $i = j$ , it is enough to use  $\eta_{LL}$ ,  $\eta_{RR}$  and  $\eta_{LR}$ . We will suppress the indices of fermion species hereafter. We may determine the scale  $\Lambda$  unambiguously by using the above form of the effective interactions; the conventional method [1] is to fix its scale by setting  $g_{\text{contact}}^2/4\pi = g_{\text{contact}}^2(\Lambda)/4\pi = 1$  for the new strong interaction coupling and by setting the largest magnitude of the coefficients  $\eta_{\alpha\beta}$  to be unity. In the following, we denote

$$\begin{aligned} \Lambda = \Lambda_{LL}^\pm & \text{ for } (\eta_{LL}, \eta_{RR}, \eta_{LR}) = (\pm 1, 0, 0) , \\ \Lambda = \Lambda_{RR}^\pm & \text{ for } (\eta_{LL}, \eta_{RR}, \eta_{LR}) = (0, \pm 1, 0) , \end{aligned}$$

$$\begin{aligned}
\Lambda &= \Lambda_{VV}^{\pm} \text{ for } (\eta_{LL}, \eta_{RR}, \eta_{LR}) = (\pm 1, \pm 1, \pm 1), \\
\Lambda &= \Lambda_{AA}^{\pm} \text{ for } (\eta_{LL}, \eta_{RR}, \eta_{LR}) = (\pm 1, \pm 1, \mp 1), \\
\Lambda &= \Lambda_{V-A}^{\pm} \text{ for } (\eta_{LL}, \eta_{RR}, \eta_{LR}) = (0, 0, \pm 1). \quad (2)
\end{aligned}$$

Such interactions can arise by interchanging constituents (when the fermions have common constituents), and/or by exchanging the binding quanta (whenever binding quanta couple to constituents of both particles).

Fermion scattering amplitude induced from the contact interaction in Eq. (1) interferes with the Standard Model (SM) amplitude destructively or constructively. The sign of interference depends on the sign of  $\eta_{\alpha\beta}$ . For instance, in the parton level  $qq \rightarrow qq$  scattering cross section in the  $\Lambda_{LL}^{\pm}$  model, the contact interaction amplitude and the SM gluon exchange amplitude interfere destructively for  $\eta_{LL} = +1$ , while they interfere constructively for  $\eta_{LL} = -1$ . In models of quark compositeness, the quark scattering cross sections induced from the contact interactions receive sizable QCD radiative corrections. Ref. 3 provides the exact next-to-leading order (NLO) QCD corrections to the contact interaction induced quark scattering cross sections.

Over the last three decades experiments at the CERN Sp $\bar{p}$ S [4,5], the Fermilab Tevatron [6,7], and the CERN LHC [8–12] have searched for quark contact interactions, characterized by the four-fermion effective Lagrangian in Eq. (1), using jet final states. These searches have been performed primarily by studying the angular distribution of the two highest transverse momentum,  $p_T$ , jets (dijets), and the inclusive jet  $p_T$  spectrum. The variable  $\chi = \exp(|(y_1 - y_2)|)$  is used to measure the dijet angular distribution, where  $y_1$  and  $y_2$  are the rapidities of the two jets with the highest transverse momenta. For collinear massless parton scattering,  $\chi$  is related to the polar scattering angle  $\theta^*$  in the partonic center-of-mass frame by  $\chi = (1 + |\cos \theta^*|)/(1 - |\cos \theta^*|)$ . The choice of  $\chi$  is motivated by the fact that the angular distribution for Rutherford scattering, which is proportional to  $1/(1 - \cos \theta^*)^2$ , is independent of  $\chi$ . In perturbative QCD the  $\chi$  distributions are relatively

flat and only mildly modified by higher-order QCD or electroweak corrections. Signatures of quark contact interactions exhibit more isotropic angular distribution than QCD and they can be identified as an excess at low values of  $\chi$ . In the inclusive jet cross section measurement, quark contact interaction effects are searched as deviations from the predictions of perturbative QCD in the tails of the high- $p_T$  jet spectrum.

Recent results from the LHC, using data collected at proton-proton center-of-mass energies of  $\sqrt{s} = 7$  and 8 TeV, extend previous Tevatron limits on quark contact interactions. Figure 1 shows the normalized dijet angular distributions for several dijet mass ranges measured in ATLAS [9] at  $\sqrt{s} = 8$  TeV. The data distributions are compared with SM predictions, estimated using PYTHIA8 [13] with GEANT4-based [14] ATLAS detector simulation and corrected to NLO QCD calculation provided by NLO Jet++ [15] including electroweak corrections [16], and with predictions including a contact interaction term in which only left-handed quarks participate at compositeness scale  $\Lambda_{LL}^+ = 8$  TeV ( $\Lambda_{LL}^- = 12$  TeV) with destructive (constructive) interference. Over a wide range of  $\chi$  and dijet mass the data are well described by the SM predictions. Using the dijet angular distributions measured at high dijet masses and  $\sqrt{s} = 8$  TeV, the ATLAS [9] and CMS [12] Collaborations have set 95% confidence level (C.L.) lower limits on the contact interaction scale  $\Lambda$ , ranging from 8.1 to 15.2 TeV for different quark contact interaction models that correspond to various combinations of  $(\eta_{LL}, \eta_{RR}, \eta_{LR})$ , as summarized in Figure 2. The contact interaction scale limits extracted using the dijet angular distributions include the exact NLO QCD corrections to dijet production induced by contact interactions [3]. In proton-proton collisions, the  $\Lambda_{LL}^\pm$  and  $\Lambda_{RR}^\pm$  contact interaction models result in identical tree-level cross sections and NLO QCD corrections and yield the same exclusion limits. For  $\Lambda_{VV}^\pm$  and  $\Lambda_{AA}^\pm$ , the contact interaction predictions are identical at tree level, but exhibit different NLO QCD corrections and yield different exclusion limits. Figure 2 also shows lower limits for two benchmark contact interaction models in which only left-handed quarks participate with destructive ( $\eta_{LL} = +1$ ) and

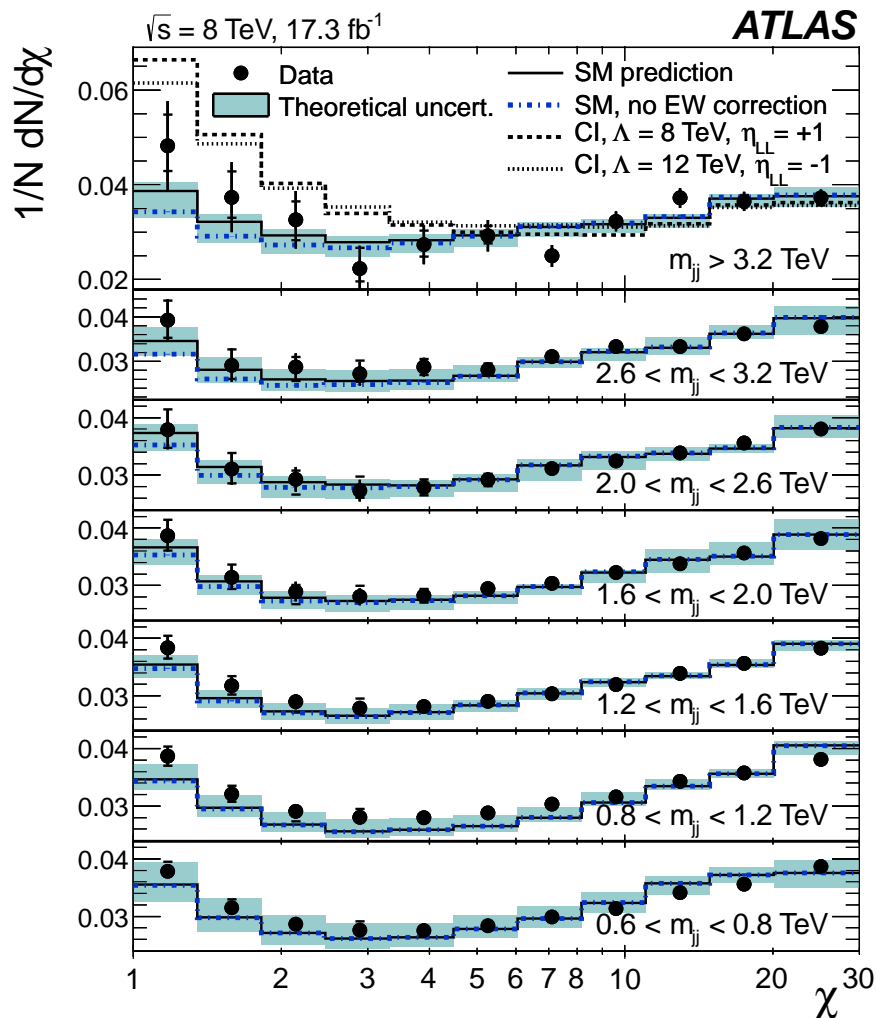


**Figure 1:** Normalized dijet angular distributions in several dijet mass ( $m_{jj}$ ) ranges. The data distributions are compared to the SM predictions (solid line) and with the predictions including a contact interaction (CI) term in which only left-handed quarks participate of compositeness scale  $\Lambda_{LL}^+ = 8 \text{ TeV}$  (dashed line) and  $\Lambda_{LL}^- = 12 \text{ TeV}$  (dotted line). The SM prediction without the electroweak (EW) corrections is also shown (blue dashed dotted line). The error bars on the data points represent statistical and experimental uncertainties combined in quadrature. The ticks on the error bars represent experimental uncertainties only. The shaded band displayed around the SM prediction shows the theoretical uncertainties. Figure adopted from Ref. 9.

constructive ( $\eta_{LL} = -1$ ) interference, using the inclusive jet  $p_T$  spectrum measured in CMS at  $\sqrt{s} = 7$  TeV [11].

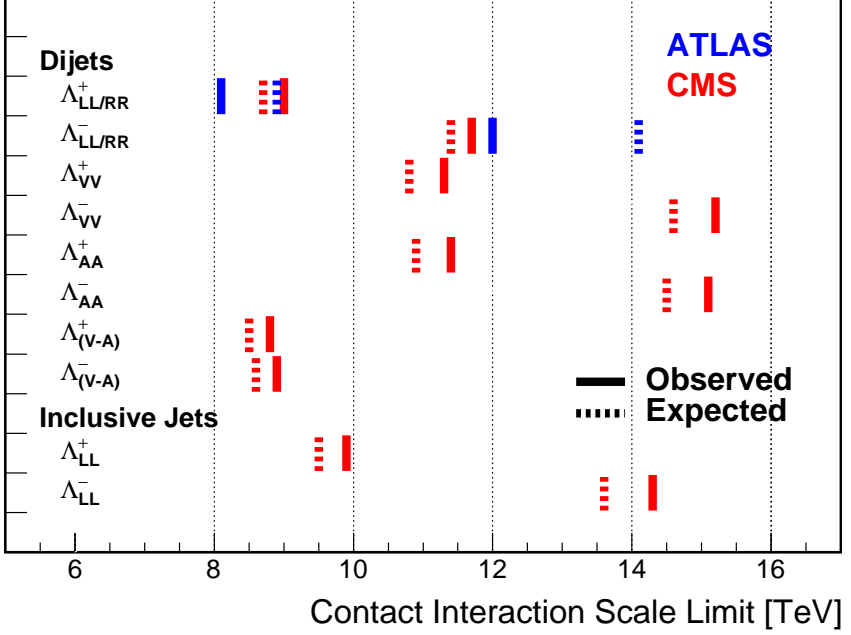


**Figure 2:** Observed (solid lines) and expected (dashed lines) 95% C.L. lower limits on the contact interaction scale  $\Lambda$  for different contact interaction models from ATLAS [9] and CMS [11,12] using the dijet angular distributions and the inclusive jet  $p_T$  spectrum. The contact interaction models used for the dijet angular distributions include the exact NLO QCD corrections to dijet production. All limits are extracted using the  $CL_s$  technique [17,18].

If leptons ( $l$ ) and quarks ( $q$ ) are composite with common constituents, the interaction of these constituents will manifest itself in the form of a  $llqq$ -type four-fermion contact interaction Lagrangian at energies below the compositeness scale  $\Lambda$ . The  $llqq$  terms in the contact interaction Lagrangian can be expressed as

$$\mathcal{L} = \frac{g_{\text{contact}}^2}{\Lambda^2} [\eta_{LL}(\bar{q}_L\gamma_\mu q_L)(\bar{l}_L\gamma^\mu l_L) + \eta_{RR}(\bar{q}_R\gamma_\mu q_R)(\bar{l}_R\gamma^\mu l_R) + \eta_{LR}(\bar{q}_L\gamma_\mu q_L)(\bar{l}_R\gamma^\mu l_R) + \eta_{RL}(\bar{q}_R\gamma_\mu q_R)(\bar{l}_L\gamma^\mu l_L)]. \quad (3)$$

Searches on quark-lepton compositeness have been reported from experiments at LEP [19–23], HERA [24,25], the Tevatron [26–30], and recently from the ATLAS [31–34] and CMS [35] experiments at the LHC. The most stringent searches for  $llqq$  contact interactions are performed by the LHC experiments using high-mass oppositely-charged lepton pairs produced through the  $q\bar{q} \rightarrow l^+l^-$  Drell-Yan process. The contact interaction amplitude of the  $u\bar{u} \rightarrow l^+l^-$  process interferes with the corresponding SM amplitude constructively (destructively) for  $\eta_{\alpha\beta} = -1$  ( $\eta_{\alpha\beta} = +1$ ). The ATLAS Collaboration has extracted limits on the  $llqq$  contact interaction for the right-right ( $\eta_{RR} = \pm 1$ ,  $\eta_{LL} = \eta_{LR} = \eta_{RL} = 0$ ), left-left ( $\eta_{LL} = \pm 1$ ,  $\eta_{RR} = \eta_{LR} = \eta_{RL} = 0$ ), and left-right ( $\eta_{LR} = \eta_{RL} = \pm 1$ ,  $\eta_{RR} = \eta_{LL} = 0$ ) models [34]. With the ATLAS full dataset at  $\sqrt{s} = 8$  TeV and combining the dielectron and dimuon channels, the 95% C.L. lower limits on the  $llqq$  contact interaction scale  $\Lambda$  are 21.1 TeV (17.5 TeV) for the right-right model, 21.6 TeV (17.2 TeV) for the left-left model, and 26.3 TeV (19.0 TeV) for the left-right model, each with constructive (destructive) interference [34]. The limits are extracted using a Bayesian approach with a prior probability flat in  $1/\Lambda^2$ . Using the dimuon channel from the 7-TeV run, the CMS Collaboration, using the  $CL_s$  technique, has set a 95% C.L. lower limit on the scale  $\Lambda$  of 13.1 TeV (9.5 TeV) for the benchmark left-left  $llqq$  contact interaction model with constructive (destructive) interference [35].

Note that the contact interactions arising from the compositeness of quarks and leptons Eq. (1) can also be regarded as a part of more general dimension six operators in the context of low energy standard model effective theory. For a complete list of these dimension six operators see Refs. 36,37.

Interactions of hypothetical dark matter candidate particles with SM can also be described as contact interactions at low energy. See “*Searches for WIMPs and Other Particles*” in this volume for limits on the interactions involving dark matter candidate particles.

## Limits on excited fermions

Another typical consequence of compositeness is the appearance of excited leptons and quarks ( $l^*$  and  $q^*$ ). Phenomenologically, an excited lepton is defined to be a heavy lepton which shares a leptonic quantum number with one of the existing leptons (an excited quark is defined similarly). For example, an excited electron  $e^*$  is characterized by a nonzero transition-magnetic coupling with electrons. Smallness of the lepton mass and the success of QED prediction for  $g - 2$  suggest chirality conservation, *i.e.*, an excited lepton should not couple to both left- and right-handed components of the corresponding lepton [38–40].

Excited leptons may be classified by  $SU(2) \times U(1)$  quantum numbers. Typical examples are:

### 1. Sequential type

$$\begin{pmatrix} \nu^* \\ l^* \end{pmatrix}_L, \quad [\nu_R^*], \quad l_R^*.$$

$\nu_R^*$  is necessary unless  $\nu^*$  has a Majorana mass.

### 2. Mirror type

$$[\nu_L^*], \quad l_L^*, \quad \begin{pmatrix} \nu^* \\ l^* \end{pmatrix}_R.$$

### 3. Homodoublet type

$$\begin{pmatrix} \nu^* \\ l^* \end{pmatrix}_L, \quad \begin{pmatrix} \nu^* \\ l^* \end{pmatrix}_R.$$

Similar classification can be made for excited quarks.

Excited fermions can be pair produced via their minimal gauge couplings. The couplings of excited leptons with  $Z$  are given by

$$\begin{aligned} & \frac{e}{2 \sin \theta_W \cos \theta_W} (-1 + 2 \sin^2 \theta_W) \bar{l}^* \gamma^\mu l^* Z_\mu \\ & + \frac{e}{2 \sin \theta_W \cos \theta_W} \bar{\nu}^* \gamma^\mu \nu^* Z_\mu \end{aligned}$$

in the homodoublet model. The corresponding couplings of excited quarks can be easily obtained. Although form factor

effects can be present for the gauge couplings at  $q^2 \neq 0$ , they are usually neglected.

Excited fermions may also be produced via the contact interactions with ordinary quarks and leptons [41]

$$\mathcal{L} = \frac{g_{\text{contact}}^2}{\Lambda^2} [\eta'_{LL}(\bar{\psi}_L\gamma_\mu\psi_L)(\bar{\psi}_L^*\gamma^\mu\psi_L^*) + (\eta''_{LL}(\bar{\psi}_L\gamma_\mu\psi_L)(\bar{\psi}_L^*\gamma^\mu\psi_L) + \text{h.c.}) + \dots] . \quad (4)$$

Again, the coefficient is conventionally taken  $g_{\text{contact}}^2 = 4\pi$ . It is widely assumed  $\eta'_{LL} = \eta''_{LL} = 1$ ,  $\eta'_{LR} = \eta''_{LR} = \eta'_{RL} = \eta''_{RL} = \eta'_{RR} = \eta''_{RR} = 0$  in experimental analyses for simplicity.

In addition, transition-magnetic type couplings with a gauge boson are expected. These couplings can be generally parameterized as follows:

$$\begin{aligned} \mathcal{L} = & \frac{\lambda_\gamma^{(\psi^*)} e}{2m_{\psi^*}} \bar{\psi}^* \sigma^{\mu\nu} (\eta_L \frac{1-\gamma_5}{2} + \eta_R \frac{1+\gamma_5}{2}) \psi F_{\mu\nu} \\ & + \frac{\lambda_Z^{(\psi^*)} e}{2m_{\psi^*}} \bar{\psi}^* \sigma^{\mu\nu} (\eta_L \frac{1-\gamma_5}{2} + \eta_R \frac{1+\gamma_5}{2}) \psi Z_{\mu\nu} \\ & + \frac{\lambda_W^{(l^*)} g}{2m_{l^*}} \bar{l}^* \sigma^{\mu\nu} \frac{1-\gamma_5}{2} \nu W_{\mu\nu} \\ & + \frac{\lambda_W^{(\nu^*)} g}{2m_{\nu^*}} \bar{\nu}^* \sigma^{\mu\nu} (\eta_L \frac{1-\gamma_5}{2} + \eta_R \frac{1+\gamma_5}{2}) l W_{\mu\nu}^\dagger \\ & + \text{h.c.}, \end{aligned} \quad (5)$$

where  $g = e/\sin\theta_W$ ,  $\psi = \nu$  or  $l$ ,  $F_{\mu\nu} = \partial_\mu A_\nu - \partial_\nu A_\mu$  is the photon field strength,  $Z_{\mu\nu} = \partial_\mu Z_\nu - \partial_\nu Z_\mu$ , *etc.*. The normalization of the coupling is chosen such that

$$\max(|\eta_L|, |\eta_R|) = 1.$$

Chirality conservation requires

$$\eta_L \eta_R = 0. \quad (6)$$

These couplings in Eq. (5) can arise from  $SU(2) \times U(1)$ -invariant higher-dimensional interactions. A well-studied model



is the interaction of homodoublet type  $l^*$  with the Lagrangian (see Refs. 42,43)

$$\mathcal{L} = \frac{1}{2\Lambda} \bar{L}^* \sigma^{\mu\nu} (gf \frac{\tau^a}{2} W_{\mu\nu}^a + g' f' Y B_{\mu\nu}) \frac{1 - \gamma_5}{2} L + \text{h.c.}, \quad (7)$$

where  $L$  denotes the lepton doublet  $(\nu, l)$ ,  $\Lambda$  is the compositeness scale,  $g, g'$  are  $SU(2)$  and  $U(1)_Y$  gauge couplings, and  $W_{\mu\nu}^a$  and  $B_{\mu\nu}$  are the field strengths for  $SU(2)$  and  $U(1)_Y$  gauge fields. These couplings satisfy the relation

$$\lambda_W = -\sqrt{2} \sin^2 \theta_W (\lambda_Z \cot \theta_W + \lambda_\gamma), \quad (8)$$

with  $\lambda_{W,Z,\gamma}$  being defined in Eq. (5) with  $\lambda_{W,Z,\gamma} = \lambda_{W,Z,\gamma}^{(\ell^*)}$  or  $\lambda_{W,Z,\gamma} = \lambda_{W,Z,\gamma}^{(\nu^*)}$ . Here  $(\eta_L, \eta_R) = (1, 0)$  is assumed. It should be noted that the electromagnetic radiative decay of  $l^*$  ( $\nu^*$ ) is forbidden if  $f = -f'$  ( $f = f'$ ).

Additional coupling with gluons is possible for excited quarks:

$$\begin{aligned} \mathcal{L} = \frac{1}{2\Lambda} \bar{Q}^* \sigma^{\mu\nu} & \left( g_s f_s \frac{\lambda^a}{2} G_{\mu\nu}^a + gf \frac{\tau^a}{2} W_{\mu\nu}^a + g' f' Y B_{\mu\nu} \right) \\ & \times \frac{1 - \gamma_5}{2} Q + \text{h.c.}, \end{aligned} \quad (9)$$

where  $Q$  denotes a quark doublet,  $g_s$  is the QCD gauge coupling, and  $G_{\mu\nu}^a$  the gluon field strength.

If leptons are made of color triplet and antitriplet constituents, we may expect their color-octet partners. Transitions between the octet leptons ( $l_8$ ) and the ordinary lepton ( $l$ ) may take place via the dimension-five interactions

$$\mathcal{L} = \frac{1}{2\Lambda} \sum_l \{ \bar{l}_8^\alpha g_8 F_{\mu\nu}^\alpha \sigma^{\mu\nu} (\eta_L l_L + \eta_R l_R) + \text{h.c.} \} \quad (10)$$

where the summation is over charged leptons and neutrinos. The leptonic chiral invariance implies  $\eta_L \eta_R = 0$  as before.

Searches for excited quarks and leptons have been performed over the last decades in experiments at the LEP [44–52], HERA [53–56], Tevatron [57–62], and LHC [63–80]. Most stringent constraints from these experiments described below are all given at 95% confidence level.

The signature of excited quarks  $q^*$  at hadron colliders is characterized by a narrow resonant peak in the reconstructed invariant mass distribution of  $q^*$  decay products. The decays via the transition-magnetic type operator in Eq. (9) are considered for excited quarks in LHC searches, and the final states to search for are dijet ( $qg$ ) [63–65, 71–74] or a jet in association with a photon ( $q\gamma$ ) [66, 67, 75] or a weak gauge boson ( $qW$ ,  $qZ$ ) [76–78]. All analyses consider only spin-1/2 excited states of first generation quarks ( $u^*$ ,  $d^*$ ) with degenerate masses, expected to be predominantly produced in proton-proton collisions, except for Ref. 74 where excited  $b$  quarks are also considered. Only the minimal gauge interactions and the transition-magnetic couplings with the form given in Eq. (9) are considered in the production process, and hence the contact interactions in Eq. (4) are not considered. The compositeness scale  $\Lambda$  is taken to be the same as the excited quark mass  $m_{q^*}$ . The transition-magnetic coupling coefficients  $f_s$ ,  $f$  and  $f'$  are assumed to be equal (denoted by  $f$ ) and around order 1.

With the full proton-proton collision data recorded at  $\sqrt{s} = 8$  TeV at LHC, the excited quark masses are excluded in dijet resonance searches up to 4.06 TeV in ATLAS [65] and 3.5 TeV in CMS [74]. Figure 3 shows the dijet mass distribution measured in CMS by using the two highest  $p_T$  jets reconstructed with the anti- $k_T$  algorithm [81] of a distance parameter of 0.5, and by combining nearby jets within  $\Delta R = \sqrt{\Delta\eta^2 + \Delta\phi^2} < 1.1$  around the leading two jets. The measured dijet mass spectrum is compared to a fit with smoothly falling background shape (solid curve) to look for a narrow resonance (3.6 TeV excited quark signal shown as one of two benchmark signals) and predictions from multi-jet events (dashed curve labeled as QCD MC) generated using PYTHIA 6.426 [82] with GEANT4-based [14] CMS detector simulation. The photon + jet resonance searches have excluded excited quarks with mass up to 3.5 TeV in both ATLAS [67] and CMS [75]. All these mass exclusions are obtained for  $f = 1$ . The  $W/Z$  boson + jet final states are examined to look for  $q^* \rightarrow q + W$  and  $q + Z$  signal in CMS [78], exploiting jet substructure technique designed to provide sensitivity for highly-boosted hadronically decaying  $W$

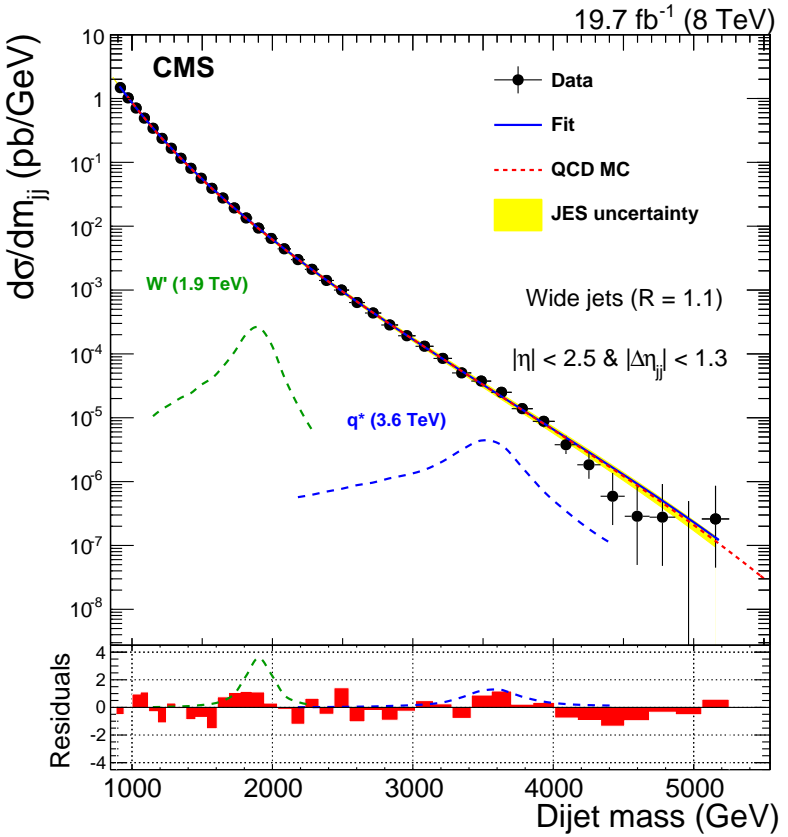


**Figure 3:** Dijet mass distribution measured by CMS using wide jets reconstructed from two highest transverse momentum jets by adding nearby jets within  $\Delta R = \sqrt{\Delta\eta^2 + \Delta\phi^2} < 1.1$ . The data distribution is compared to a fit representing a smooth background spectrum (solid curve) and to the normalized prediction of multi-jet background simulated by PYTHIA (labeled as QCD MC). Excited quark signal with mass of 3.6 TeV is also shown for comparison. Shown at the bottom panel is the bin-by-bin fit residuals normalized by the statistical uncertainty of the data. Figure adopted from Ref. 74.

and  $Z$  bosons. The  $q^*$  mass exclusion of 3.2 (2.9) TeV is obtained from the  $W + \text{jet}$  ( $Z + \text{jet}$ ) search.

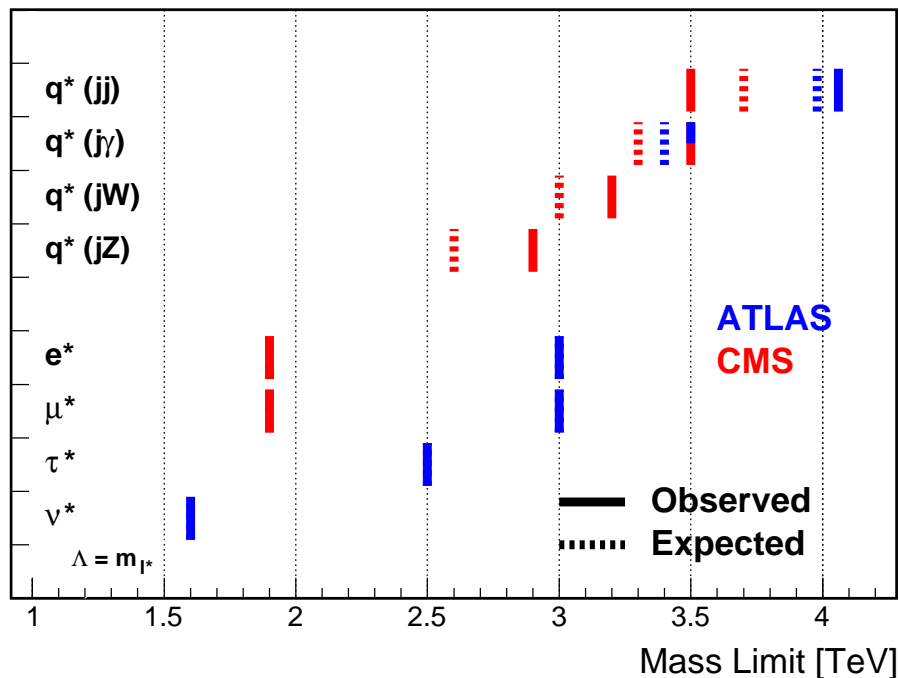


**Figure 4:** 95% C.L. lower mass limits for the excited quarks and leptons at ATLAS [65,67,69,70] and CMS [74,75,78,80] experiments. Shown are the most stringent limits for each excited fermion from both experiments. Only first generation quarks ( $u$ ,  $d$ ) with transition-magnetic type interactions with  $f_s = f = f' = 1$  are considered for excited quarks, and the limits are shown for different final states denoted in parentheses. Excited lepton limits are given for contact interactions with  $\Lambda = m_{l^*}$ . The observed limit from  $q^* \rightarrow q + \gamma$  is 3.5 TeV for both ATLAS and CMS. For the excited leptons the observed and expected limits are same in both ATLAS and CMS.

Searches for excited leptons  $l^*$  are also performed at the LHC using proton-proton collision data recorded at  $\sqrt{s} = 7$  and 8 TeV [68–70,79,80]. Considering the single  $l^*$  production Eq. (4) and electromagnetic radiative decay to a SM lepton ( $l$ ) and a photon ( $\gamma$ ), both the excited electron and excited muon masses below 2.2 TeV are excluded for  $\Lambda = m_{l^*}$  at  $\sqrt{s} = 8$  TeV in ATLAS [69]. With the full data at  $\sqrt{s} = 8$  TeV, the inclusive search on multi-lepton signatures with 3 or more charged leptons in ATLAS [70] further constrains the excited

charged leptons and neutrinos. Considering both the transition-magnetic Eq. (7) and contact interaction Eq. (4) processes, the lower mass limits for the  $e^*$ ,  $\mu^*$ ,  $\tau^*$  and  $\nu^*$  (for every excited neutrino flavor) are obtained to be 3.0, 3.0, 2.5 and 1.6 TeV, respectively, for  $\Lambda = m_{e^*}$ ,  $m_{\mu^*}$ ,  $m_{\tau^*}$  and  $m_{\nu^*}$ . The rate of pair-produced excited leptons is independent of  $\Lambda$  for the minimal gauge interaction processes, and it allows to improve the search sensitivity with multi-lepton signatures at high  $\Lambda$ , especially for excited neutrinos because the predominant  $\nu_l^* \rightarrow l + W$  decays result in a higher acceptance for  $\geq 3$  charged lepton final states. A similar search for excited leptons with  $l^* \rightarrow l + \gamma$  decays ( $l = e, \mu$ ) produced in contact interactions is performed by the CMS Collaboration at  $\sqrt{s} = 7$  TeV [80], resulting in a mass exclusion of 1.9 TeV for  $\Lambda = m_{l^*}$ . Figure 4 summarizes the most stringent 95% C.L. lower mass limits for the excited quarks and leptons obtained from the LHC experiments.

## References

1. E.J. Eichten, K.D. Lane, and M.E. Peskin, Phys. Rev. Lett. **50**, 811 (1983).
2. E.J. Eichten *et al.*, Rev. Mod. Phys. **56**, 579 (1984); Erratum *ibid.* **58**, 1065 (1986).
3. J. Gao *et al.*, Phys. Rev. Lett. **106**, 142001 (2011).
4. G. Arnison *et al.* [UA1 Collab.], Phys. Lett. **B177**, 244 (1986).
5. J.A. Appel *et al.* [UA2 Collab.], Phys. Lett. **B160**, 349 (1985).
6. F. Abe *et al.* [CDF Collab.], Phys. Rev. Lett. **62**, 613 (1989);  
F. Abe *et al.* [CDF Collab.], Phys. Rev. Lett. **69**, 2896 (1992);  
F. Abe *et al.* [CDF Collab.], Phys. Rev. Lett. **77**, 5336 (1996);  
F. Abe *et al.* [CDF Collab.], Erratum Phys. Rev. Lett. **78**, 4307 (1997).
7. B. Abbott *et al.* [DØ Collab.], Phys. Rev. Lett. **80**, 666 (1998);  
B. Abbott *et al.* [DØ Collab.], Phys. Rev. Lett. **82**, 2457 (1999);  
B. Abbott *et al.* [DØ Collab.], Phys. Rev. **D62**, 031101 (2000);

- B. Abbott *et al.* [DØ Collab.], Phys. Rev. **D64**, 032003 (2001);  
B. Abbott *et al.* [DØ Collab.], Phys. Rev. Lett. **103**, 191803 (2009).
8. G. Aad *et al.* [ATLAS Collab.], Phys. Rev. **B694**, 327 (2011);  
G. Aad *et al.* [ATLAS Collab.], New J. Phys. **13**, 053044 (2011);  
G. Aad *et al.* [ATLAS Collab.], JHEP **1301**, 029 (2013).
9. G. Aad *et al.* [ATLAS Collab.], Phys. Rev. Lett. **114**, 221802 (2015).
10. V. Khachatryan *et al.* [CMS Collab.], Phys. Rev. Lett. **105**, 262001 (2010);  
V. Khachatryan *et al.* [CMS Collab.], Phys. Rev. Lett. **106**, 201804 (2011);  
S. Chatrchyan *et al.* [CMS Collab.], JHEP **1205**, 055 (2012).
11. S. Chatrchyan *et al.* [CMS Collab.], Phys. Rev. **D87**, 052017 (2013).
12. V. Khachatryan *et al.* [CMS Collab.], Phys. Lett. **B746**, 79 (2015).
13. T. Sjöstrand, S. Mrenna, and P. Skands, Comp. Phys. Comm. **178**, 852 (2008).
14. S. Agostinelli *et al.* [GEANT4 Collab.], GEANT4: a simulation toolkit, Nucl. Instrum. Methods **A506**, 250 (2003).
15. Z. Nagy, Phys. Rev. Lett. **88**, 122003 (2002);  
Z. Nagy, Phys. Rev. **D68**, 094002, (2003).
16. S. Dittmaier, A. Huss, and C. Speckner, JHEP **1211**, 095 (2012).
17. T. Junk, Nucl. Instrum. Methods **A434**, 435 (1999).
18. A. L. Read, J. Phys. **G28**, 2693 (2002).
19. S. Schael *et al.* [ALEPH Collab.], Eur. Phys. J. **C49**, 411 (2007).
20. J. Abdallah *et al.* [DELPHI Collab.], Eur. Phys. J. **C45**, 589 (2006).
21. M. Acciarri *et al.* [L3 Collab.], Phys. Lett. **B489**, 81 (2000).
22. K. Ackerstaff *et al.* [OPAL Collab.], Phys. Lett. **B391**, 221 (1997).
23. G. Abbiendi *et al.* [OPAL Collab.], Eur. Phys. J. **C33**, 173 (2004).
24. F.D. Aaron *et al.* [H1 Collab.], Phys. Lett. **B705**, 52 (2011).

25. S. Chekanov *et al.* [ZEUS Collab.], Phys. Lett. **B591**, 23 (2004).
26. F. Abe *et al.* [CDF Collab.], Phys. Rev. Lett. **68**, 1463 (1992).
27. F. Abe *et al.* [CDF Collab.], Phys. Rev. Lett. **79**, 2198 (1997).
28. T. Affolder *et al.* [CDF Collab.], Phys. Rev. Lett. **87**, 231803 (2001).
29. A. Abulencia *et al.* [CDF Collab.], Phys. Rev. Lett. **96**, 211801 (2006).
30. B. Abbott *et al.* [DØ Collab.], Phys. Rev. Lett. **82**, 4769 (1999).
31. G. Aad *et al.* [ATLAS Collab.], Phys. Rev. **D84**, 011101 (2011).
32. G. Aad *et al.* [ATLAS Collab.], Phys. Lett. **B712**, 40 (2012).
33. G. Aad *et al.* [ATLAS Collab.], Phys. Rev. **D87**, 015010 (2013).
34. G. Aad *et al.* [ATLAS Collab.], Eur. Phys. J. **C74**, 3134 (2014).
35. S. Chatrchyan *et al.* [CMS Collab.], Phys. Rev. **D87**, 032001 (2013).
36. W. Buchmuller and D. Wyler, Nucl. Phys. **B268**, 621 (1986).
37. B. Grzadkowski *et al.*, JHEP **1010**, 085 (2010).
38. F.M. Renard, Phys. Lett. **B116**, 264 (1982).
39. F. del Aguila, A. Mendez, and R. Pascual, Phys. Lett. **B140**, 431 (1984).
40. M. Suzuki, Phys. Lett. **B143**, 237 (1984).
41. U. Baur, M. Spira, and P.M. Zerwas, Phys. Rev. **D42**, 815 (1990).
42. K. Hagiwara, D. Zeppenfeld, and S. Komamiya, Z. Phys. **C29**, 115 (1985).
43. N. Cabibbo, L. Maiani, and Y. Srivastava, Phys. Lett. **B139**, 459 (1984).
44. D. Decamp *et al.* [ALEPH Collab.], Phys. Reports **216**, 253 (1992).
45. P. Barate *et al.* [ALEPH Collab.], Eur. Phys. J. **C4**, 571 (1998).
46. P. Abreu *et al.* [DELPHI Collab.], Nucl. Phys. **B367**, 511 (1991).

47. J. Abdallah *et al.* [DELPHI Collab.], *Eur. Phys. J.* **C37**, 405 (2004).
48. O. Adriani *et al.* [L3 Collab.], *Phys. Reports* **236**, 1 (1993).
49. P. Achard *et al.* [L3 Collab.], *Phys. Lett.* **B531**, 28 (2002).
50. P. Achard *et al.* [L3 Collab.], *Phys. Lett.* **B568**, 23 (2003).
51. G. Abbiendi *et al.* [OPAL Collab.], *Phys. Lett.* **B544**, 57 (2002).
52. G. Abbiendi *et al.* [OPAL Collab.], *Phys. Lett.* **B602**, 167 (2004).
53. C. Adloff *et al.* [H1 Collab.], *Phys. Lett.* **B525**, 9 (2002).
54. F.D. Aaron *et al.* [H1 Collab.], *Phys. Lett.* **B663**, 382 (2008).
55. F.D. Aaron *et al.* [H1 Collab.], *Phys. Lett.* **B666**, 131 (2008).
56. S. Chekanov *et al.* [ZEUS Collab.], *Phys. Lett.* **B549**, 32 (2002).
57. D. Acosta *et al.* [CDF Collab.], *Phys. Rev. Lett.* **94**, 101802 (2005).
58. A. Abulencia *et al.* [CDF Collab.], *Phys. Rev. Lett.* **97**, 191802 (2006).
59. T. Aaltonen *et al.* [CDF Collab.], *Phys. Rev.* **D79**, 112002 (2009).
60. V.M. Abazov *et al.* [DØ Collab.], *Phys. Rev.* **D73**, 111102 (2006).
61. V.M. Abazov *et al.* [DØ Collab.], *Phys. Rev.* **D77**, 091102 (2008).
62. V.M. Abazov *et al.* [DØ Collab.], *Phys. Rev. Lett.* **103**, 191803 (2009).
63. G. Aad *et al.* [ATLAS Collab.], *Phys. Lett.* **B708**, 37 (2012).
64. G. Aad *et al.* [ATLAS Collab.], *JHEP* **1301**, 29 (2013).
65. G. Aad *et al.* [ATLAS Collab.], *Phys. Rev.* **D91**, 052007 (2015).
66. G. Aad *et al.* [ATLAS Collab.], *Phys. Rev. Lett.* **108**, 211802 (2012).
67. G. Aad *et al.* [ATLAS Collab.], *Phys. Lett.* **B728**, 562 (2014).
68. G. Aad *et al.* [ATLAS Collab.], *Phys. Rev.* **D85**, 072003 (2012).
69. G. Aad *et al.* [ATLAS Collab.], *New J. Phys.* **15**, 093011 (2013).
70. G. Aad *et al.* [ATLAS Collab.] *JHEP* **1508**, 138 (2015).



71. S. Chatrchyan *et al.* [CMS Collab.], Phys. Lett. **B704**, 123 (2011).
72. S. Chatrchyan *et al.* [CMS Collab.], JHEP **1301**, 13 (2013).
73. S. Chatrchyan *et al.* [CMS Collab.], Phys. Rev. **D87**, 114015 (2013).
74. V. Khachatryan *et al.* [CMS Collab.], Phys. Rev. **D91**, 052009 (2015).
75. V. Khachatryan *et al.* [CMS Collab.], Phys. Lett. **B738**, 274 (2014).
76. S. Chatrchyan *et al.* [CMS Collab.], Phys. Lett. **B722**, 28 (2013).
77. S. Chatrchyan *et al.* [CMS Collab.], Phys. Lett. **B723**, 280 (2013).
78. V. Khachatryan *et al.* [CMS Collab.], JHEP **1408**, 173 (2014).
79. S. Chatrchyan *et al.* [CMS Collab.], Phys. Lett. **B704**, 143 (2011).
80. S. Chatrchyan *et al.* [CMS Collab.], Phys. Lett. **B720**, 309 (2013).
81. M. Cacciari, G.P. Salam, and G. Soyez, JHEP **0804**, 063 (2008).
82. T. Sjöstrand *et al.*, Comp. Phys. Comm. **135**, 238 (2001).